First Accuracy Evaluation of NIST-F2

First Accuracy Evaluation of NIST-F2

Thomas P. Heavner[1], Elizabeth A. Donley[1], Filippo Levi[2], Giovanni Costanzo [3], Thomas E. Parker[1], Jon H. Shirley[1], Neil Ashby[1], Stephan Barlow[1], S. R. Jefferts[1]

[1] Time and Frequency Division, National Institute of Standards and Technology, Boulder, CO, 80305, USA

[2] Istituto Nazionale di Ricerca Metrologica, INRIM, Strada delle Cacce 91, 10135 Torino, Italy

[3] Politecnico di Torino, C. Duca degli Abruzzi 24 10129 Torino , Italy

Abstract

We report the first accuracy evaluation of NIST-F2, a second-generation laser-cooled Cesium fountain primary standard developed at the National Institute of Standards and Technology (NIST) with a cryogenic (Liquid Nitrogen) microwave cavity and flight region. The 80 K atom interrogation environment reduces the uncertainty due to the Blackbody Radiation (BBR) shift by more than a factor of 50. Also, the Ramsey microwave cavity exhibits a high Q (>50,000) at this low temperature, resulting in a reduced distributed cavity phase shift. NIST-F2 has undergone many tests and improvements since we first began operation in 2008. In the last few years NIST-F2 has been compared against a NIST maser time scale and NIST-F1 (the US primary frequency standard) as part of in-house accuracy evaluations. We report the results of nine in-house comparisons since 2010 with a focus on the most recent accuracy evaluation. This paper discusses the design of the physics package, the laser and optics systems, and the accuracy evaluation methods. The Type B fractional uncertainty of NIST-F2 is shown to be 0.11×10^{-15} and is dominated by microwave amplitude dependent effects. The most recent evaluation (August 2013) had a statistical (Type A) fractional uncertainty of 0.44×10^{-15}.

---

1. Introduction

The Time and Frequency Division of the National Institute of Standards and Technology (NIST) in Boulder, CO has operated NIST-F1, a laser-cooled cesium (Cs) fountain primary frequency standard, since 1998 [1,2]. Currently, the type B fractional uncertainty in NIST-F1 is 0.31×10^{-15} and is dominated by the uncertainty in the blackbody radiation (BBR) shift correction, which is 0.28×10^{-15} (this corresponds to a 1 degree uncertainty in the radiation environment as seen by the atoms in NIST-F1) . To improve the performance of the NIST primary frequency standard, we needed to reduce the uncertainty due to the BBR effect. To accomplish this goal and to better understand the accepted model of the BBR shift, we developed NIST-F2, a laser-cooled Cs fountain primary frequency standard in which the microwave cavity structure and flight tube operate at cryogenic temperatures (80 K).

The total fractional frequency bias due to the BBR shift in NIST-F2 is less than 1×10^{-16}

and this allows for a direct measurement of the effect in NIST-F1. Operation of a fountain at cryogenic temperatures has additional advantages as well as challenges due to the high Q of the 80 K Ramsey microwave cavity. The high Q reduces the distributed cavity phase shift (DCPS), which is a significant source of uncertainty in many Cs primary frequency standards. On the negative side, the high Q creates cavity pulling bias concerns if the cavity resonance is not sufficiently close to the atomic resonance.

There has been much progress in the area of cesium fountain frequency standards, particularly in the area of methods to measure distributed cavity phase shifts (DCPS) [3], resulting in many groups now reporting Type B uncertainties in the range of (2-3) × 10^{-16} [4] with a recent publication by the National Physical Laboratory (NPL) group reporting the lowest Type B for Cs fountains of 2.3 × 10^{-16} [5]. It is difficult to significantly reduce the uncertainty due to the BBR shift in room temperature Cs fountains using leveraged temperature measurements. For example, changing the temperature of the microwave cavity structure only a few degrees at room temperature does not significantly change the BBR shift but does cause the Ramsey cavity to move away from resonance, thus introducing microwave amplitude and cavity pulling effects.

The design concepts for NIST-F2 were first presented in 2003 [6] and in some more detail in 2005 [7]. Two identical physics packages were constructed and assembled at NIST in Boulder, CO. One resides at NIST and the second was delivered to the Istituto Nazionale di Ricerca Metrologica (INRIM) in Turin, Italy [8]. Clock transitions and preliminary results were first presented in 2008 [9]. In the last several years, we have worked on improving the stability and characterizing the accuracy of NIST-F2. Figure 1 shows the Allan deviation of NIST-F2, illustrating a stability of ≈1.7 × $10^{-13}\tau^{-1/2}$.

Here we present measurements from September 2010 to August 2013. Many systematic biases are evaluated repeatedly in NIST-F2 (as well as NIST-F1), so the Type B uncertainties vary during this period. For example, the microwave power shift reported in this paper is from measurements in November 2012. However, since the microwave synthesizer was slightly modified shortly before this paper was written, the microwave power shift measurements were repeated (resulting in slightly larger uncertainties) for the August 2013 measurements, which will be submitted to the BIPM for inclusion into *Circular-T*.

The NIST-F2 apparatus is described in section 2 of this paper. The evaluation procedures and systematic biases are outlined in section 3. Section 4 presents the results of the accuracy evaluations of NIST-F2, which are performed using the NIST maser based time scale and NIST-F1 as references.

2. NIST-F2 Apparatus

2.1 Physics Package

The design, operating principles, and preliminary results from NIST-F2 have been discussed in a previous publication [10]. The physics package, shown in Figure 2, consists of a combined cold atom source and detection chamber which is attached to a copper microwave cavity structure within a liquid nitrogen (LN_2) dewar.

The cooling/detection chamber has six windows in the (1, 1, 1) configuration for cooling and launching atoms. Additional ports and windows in the mid-plane provide access for the repump laser, cameras and Cesium ovens. The detection region has two (upper and lower) zones with identical geometry. Each has a half-spherical mirror within the vacuum chamber for light collection. The mirror faces a re-entrant window against which a detector module is located. The detector module contains light collecting optics, a photodiode and an amplifier. Additional windows allow access for detection, blast and re-pump beams. The composite chamber design minimizes the distance between the atom cooling region and the microwave interrogation region.

Above the source/detection chamber is a LN_2 dewar within an insulating vacuum chamber. The copper microwave cavity and flight tube structure are mounted on a cold plate that in turn is attached to the LN_2 dewar. The C-field and three layers of magnetic shields reside within the LN_2 dewar vacuum chamber.

The top flange of the LN_2 dewar houses feedthroughs for microwave signals, temperature sensors, LN_2 fill lines, wiring for the C-field, coils to generate transverse magnetic fields, shim coils and the magnetic shield degauss system.

The LN_2 level in the dewar is controlled by an automatic system. Because the Ramsey cavity is not exactly on resonance at the nominal temperature provided by the LN_2 dewar, it is necessary to pump on the volume above the LN_2, thus lowering the temperature of the LN_2 bath, to bring the cavity into resonance. The long-term temperature of the Ramsey cavity structure is controlled by a programmable servo system that monitors the pressure above the LN_2 temperature and opens and closes a valve to a pump to stabilize the pressure. Figure 3 shows the Allan deviation of the temperature of the Ramsey cavity over 14 days.

While many of the NIST-F2 parameters are varied in the accuracy evaluation process, typically the optical molasses load time is ≈ 0.2 s, the atom temperature is < 1 μK, the Ramsey time is ≈ 0.6 s, and the C-field is ≈ 2.5 mG (250 nT).

2.2 Laser and Optics

The laser system for NIST-F2 is based on a commercial titanium sapphire ring laser pumped by a high-power diode system operating at 532 nm. This provides about 1 Watt of 852 nm of light with a linewidth of 50 kHz. This light is delivered via a polarization maintaining (PM) optical fiber cable to a network of six double-pass AOM assemblies, which generate the six independent cooling and launching beams[11]. The output beam of each individual AOM assembly is injected into a PM fiber, which travels to the physics package. Six output collimators are attached to the vacuum chamber at the re-entrant windows at the source region. Each output collimator has a beam pick off that directs a small amount of light onto a photo-detector. The six photo-detector signals from the collimators are used in a servo control system whereby the light levels during molasses, launch, post-cool, and launch are controlled by adjusting the RF power delivered to each corresponding AOM.

2.3 Microwave Synthesis

NIST-F2 uses the same microwave synthesis architecture as NIST-F1 [1]. A high-performance quartz oscillator is locked (≈10 s time constant) to a reference signal from a maser in the NIST time scale. This signal is used to make 100 MHz using a multiplier chain which in turn is fed to a dielectric resonator oscillator (DRO) to make 9.200 GHz. A single-sideband mixer is used with a computer-controlled DDS signal at 7.368 MHz to make 9.1926 GHz to drive clock transitions. This system has been described in detail in previous work and has the performance to support the stability and accuracy of the fountains [1].

2.4 NIST Maser Time scale

A NIST maser-based time scale serves as a flywheel reference during the long evaluation intervals of NIST-F2 (and NIST-F1). The effective use of this time scale and deadtime issues are discussed in [12]. Additionally, if both fountains are running simultaneously, we are able to use the well characterized accuracy of NIST-F1 as a reference for NIST-F2.

3. NIST-F2 Systematic Biases

3.1 Relativistic Effects

The gravitational redshift in Boulder, CO is a large systematic frequency bias for both NIST-F2 and NIST-F2. This bias has been well studied for NIST-F1 [13], and because NIST-F2 is located in an adjacent laboratory on the same floor as NIST-F1, we can easily correct for this bias. Since this is a relativistic effect, our correction here includes the second-order Doppler effect contribution. The total fractional correction due to relativity (gravitational redshift and second-order Doppler) for NIST-F2 is $(+179.87 \pm 0.02) \times 10^{-15}$.

3.2 Second-Order Zeeman

We use a similar method as with NIST-F1 [2] to measure the second-order Zeeman shift. First, the magnetic field along the flight tube is mapped by launching the atoms to various apogees, typically in 1 cm increments. A low frequency (≈1 kHz) transverse magnetic field is turned on for 100 ms at apogee to drive the $|3, 0\rangle \rightarrow |3, 1\rangle$ transition. This process generates a map of the magnetic field along the vertical axis of the flight tube. The map is then integrated with respect to the ballistic trajectory of the atom cloud to predict the central fringe on the $|3, 1\rangle \rightarrow |4, 1\rangle$ magnetic field-sensitive manifold as a function of launch height. This prediction is then compared with measurements of the $|3, 1\rangle \rightarrow |4, 1\rangle$ Ramsey fringes for various launch heights. Using this method we are able to unambiguously identify the central field sensitive fringe.

In NIST-F2 we have concerns about the adequacy of shielding and the possibility of losing identity of this central fringe during long evaluation campaigns. So, we also measure magnetic field transitions approximately every 10^3 s during standard operation. To achieve this, we employ a two-stage magnetic field line servo. First, by use of the same magnetic field coils along the flight tube as described above, a low frequency field transverse to the C-Field axis excites the $|3, 0\rangle \rightarrow |3, 1\rangle$ transition not only at apogee but continuously during the trajectory of the atoms [14]. The resonance is measured by use of a square wave servo (the same method used to measure the clock transition). This provides a measurement of the average magnetic

field as seen by the atoms during their trajectory. While this measurement does not allow for an accurate second-order Zeeman correction, it does provide enough precision to generate an initial guess for the control software to find and lock on the central fringe on the |3, 1> → |4, 1> manifold. This is the second stage of the magnetic field measurement servo. Thus, we have a good record of small magnetic field fluctuations in the time domain and are able to apply the second-order Zeeman correction in near real-time.

Figure 4 is the Allan deviation of magnetic field measurements over a six day interval during standard NIST-F2 operation.

We assign an uncertainty in the measurement of the |3, 1> →|4, 1> central fringe of ± 6 % of a fringe spacing, which corresponds to a fractional uncertainty of 0.03×10^{-15} in the second-order Zeeman correction. This uncertainty is primarily set by software parameters in the magnetic field servo and can be improved in the future with modifications to the routines.

The NIST-F2 field map is also used to estimate any bias due to magnetic field inhomogeneity using the theory in [15] and is found to be $< 1 \times 10^{-17}$.

3.3 Spin-Exchange Shift

The spin-exchange shift is evaluated by operating NIST-F2 over a range of atomic densities while using the NIST maser timescale or NIST-F1 as a local oscillator reference. Variations in the atomic density are achieved by making small changes to the molasses load time, state–selection amplitude, or Cs oven temperature. As described elsewhere [12], the spin-exchange shift is a systematic bias that is evaluated using the statistics of frequency measurements. Thus it is included with the Type A uncertainty, but it is included in the list of other Type B uncertainties for completeness and the bias is shown only for one atomic density. In other words, there is no single spin-exchange shift correction since NIST-F2 operates over a range of atomic densities. However, a small uncertainty (Type B) in the spin-exchange shift is due to nonlinear effects in the variations in the atomic density in NIST-F2.

A typical fractional frequency shift in NIST-F2 operating at low density due to the spin-exchange bias is $(-0.71 \pm 0.24) \times 10^{-15}$ and the nonlinear effects are included as Type B with an uncertainty of 0.02×10^{-15}.

3.4 Blackbody Radiation (BBR) Shift

Since the Cs clock transition is evaluated in a cryogenic microwave cavity and flight tube (approximately 80 K) the total BBR bias in NIST-F2 is $<10^{-16}$.

The temperature of the NIST-F2 microwave cavity and flight tube structure is measured using platinum RTDs at several locations along the length. A small amount of room temperature (300 K) radiation enters the flight tube through a vacuum window located below the optical molasses region. However, a light baffle structure between the source chamber and the microwave cavities reduces the amount of room temperature radiation that scatters up the flight tube. We model the effect of this window and the temperature gradient to find an effective temperature, T_{eff}, as experienced by the atoms along the ballistic trajectory to estimate the BBR shift in NIST-F2.

The BBR fractional shift in Cs is given by

$$\frac{\Delta\omega}{\omega_0} = \beta\left(\frac{T_{eff}}{300\ K}\right)^4\left[1 + \varepsilon\left(\frac{T_{eff}}{300\ K}\right)^2\right]. \qquad (1)$$

Using accepted values of $\beta = (-1.710 \pm 0.006) \times 10^{-14}$ and $\varepsilon = 0.013 \pm 0.001$, we determine the fractional Blackbody shift for NIST-F2 to be (-0.087±0.005) × 10^{-15}. The uncertainty in T_{eff} is ± 1 K and has a negligible contribution at ≈ 80 K.

3.5 Microwave Effects

Effects that are known to have microwave power dependent biases include spurious terms in the microwave field [16], microwave leakage [17], distributed cavity phase shifts [18,19], and the microwave lensing effect [20,21]. In NIST-F2, we evaluate many of these effects by a variety of means. Unfortunately it is essentially impossible to cleanly separate all of the above effects by a simple sequence of measurements. We therefore discuss each of these effects separately and then finally discuss the overall microwave effects in the error budget of the standard.

3.51 Distributed Cavity Phase Shift (DCPS)

As we first pointed out in [18] the distributed cavity phase shift (DCPS) is power dependent. The groups at Penn State and Observatoire de Paris later extended our analysis in [22, 3]. This has led to a significant improvement in the understanding of the DCPS in fountain standards. Using the notation in [3] we can analyze the frequency shift induced by the various normal modes. In NIST-F2, the cavity Q is quite high (Q > 50,000) and the cavity is basically unloaded (insertion loss ≈55 dB). The m = 0 DCPS, which is essentially a longitudinal phase shift, has an amplitude considerably less than $\frac{\delta\omega}{\omega_0} < 1 \times 10^{-18}$ under normal operational conditions. The two orthogonal m = 1 modes are excited in superposition in the NIST-F2 cavity due to the geometry of the four feeds. Because the loaded (measured) cavity Q is essentially that predicted by theory, we can largely exclude shifts due to inhomogeneous wall resistivity, or imbalances due to feed reflectivity. Cavity feeds are balanced in both phase $(\delta\varphi \leq 75\ \mu rad)$ and amplitude $(\frac{\delta b}{b} \leq -60\ dB)$, and the detection system has been carefully designed to minimize vignetting. Additionally, the measured tilt sensitivity of the NIST-F2 cavity when driving one microwave feed versus the opposite feed indicates the fountain verticality to be within 100 µrad, consistent with both the design verticality of 100 µrad, and the mechanically measured verticality of 20 µrad. Figure 5 shows the results of these measurements taken at various tilt angles along one axis and microwave power levels. Note that measurements were made as the fountain was tilted with respect to two orthogonal axes and the results decomposed into tilt sensitivities for the two m = 1 modes. The resulting m = 1 tilt sensitivities predict no frequency shift with an uncertainty of $\frac{\delta\omega}{\omega} = 2 \times 10^{-17}$ for each mode. We have also measured the tilt sensitivity with both feeds driven, which also results in no measureable frequency shift at the $\frac{\delta\omega}{\omega} = 2 \times 10^{-17}$ level of uncertainty for normal operation. Unlike the typical case for a two-feed cavity, the m = 2 mode is essentially unexcited in this cavity, and the frequency shift associated with m = 2 is therefore suppressed, with the result that the predicted m = 2 DCPS is $\frac{\delta\omega}{\omega} \leq 2 \times 10^{-17}$. These results are summarized in the uncertainty budget.

3.52 Microwave Leakage

Microwave leakage can occur in two distinct ways in a state-selected atomic fountain; either between the two Ramsey pulses (e.g. above the microwave cavity), or after the second Ramsey pulse (below the microwave cavity) [17]. In NIST-F2 the drift tube above the microwave cavity is a circular waveguide that is shorted at the upper end. The length is carefully chosen to be anti-resonant at the 9.1926 GHz clock transition frequency, and the only propagating mode is a TE_{11} mode, which should not be excited by the cavity mode and in any case should cause no frequency shift to first-order. This leaves the possibility of leakage below the microwave cavity, which has a characteristic signature with microwave amplitude of maximizing (with alternating sign) at odd $\pi/2$ excitation levels and generally scaling with excitation level. The test for this behavior is discussed below.

3.53 Microwave Spurious Spectrum Effects

We have measured the spectrum of the synthesizer, which is generally very similar to that described in [23], and, along with the theory presented in [16] conclude that any frequency bias caused by the microwave spectrum is smaller than $\frac{\delta f}{f} = (0 \pm 0.05) \times 10^{-15}$. This does not include effects of pulsed operation as discussed in [16] and as measured using the apparatus described by Santarelli [24].

3.54 Microwave Lensing

This shift is discussed in [20]; unfortunately the theory presented in this paper has several errors and corrections are not available in the literature. We have significantly extended and corrected the ideas presented in [20] including a full treatment of the atomic wave packet behavior in [21]. In NIST-F2, under normal operating conditions, any microwave lensing shift scales just like the microwave leakage shift and is therefore treated below.

3.55 Generalized Power Dependence

As discussed above, we measure the frequency shift of NIST-F2 as a function of microwave amplitude to look for this family of frequency biases, which depend on the microwave field amplitude. The first-order behavior for many of the effects can be approximated by

$$\frac{\delta\omega}{\omega o} = A\, n \sin(\frac{n\pi}{2}) \qquad . \qquad (2)$$

Here, *A* gives the magnitude of the bias, the excitation level is assumed to be such that $b\tau = \frac{n\pi}{2}$ for *n*=1,3,5,7..., and $\frac{\delta\omega(\frac{\pi}{2})}{\omega o}$ is the fractional frequency shift at normal optimal power. Given the cloud size and temperature in NIST-F2 as well as other factors such as toss height and aperture size and placement, the effects that scale in this fashion include microwave leakage, parts of the DCPS and microwave lensing. Second-order effects in the leakage shift leading to quadratic behavior can, under some circumstances, be as large (or larger) than the first-order effect [25]. In the case of NIST-F2 with the cloud sizes, atom temperatures and apertures that apply, the frequency shift vs. microwave amplitude is strongly dominated by effects described by Equation 2 above. When we fit the data in Fig. 6 to the shift given by Equation 2 we determine the shift at normal operational power $\left(\frac{\pi}{2}\right)$ to be $\frac{\delta f}{f} = (-0.006 \pm 0.08) \times$

10^{-15}; the dotted line in Fig. 6 is the fitted shift with an amplitude given by the uncertainty in the fit. Other microwave frequency shifts (*m* = 0 DCPS for example) are evaluated theoretically and called out separately in the uncertainty budget shown in Table 1.

3.6 Other Frequency Biases

3.61 First and Second-Order Cavity Pulling

The temperature of the NIST-F2 Ramsey cavity changes slightly due to changes in the LN_2 level and the limitations of our liquid fill and temperature-control system. This in turn causes changes in the resonant frequency of the microwave cavity. While cavity pulling in NIST-F1, for example, is considered in the list of uncorrected biases, it is insignificant because it is straightforward to keep the cavity close to resonance such that cavity pulling effects vanish.

The temperature of the NIST-F2 Ramsey cavity is logged every 30 s, and by analyzing this record we determine the cavity is on average detuned 79.4 kHz from resonance.

Using the model developed in [26] we estimate any fractional frequency bias due to first-order cavity pulling to be $<10^{-18}$. While the Q of our cavity is high, the density of Cs atoms launched is sufficiently low to make this effect negligible.

Second-order cavity pulling is estimated using the expression found in [27]. The microwave power in NIST-F2 is set within ≈0.3 dBm of optimum power. This gives the magnitude of the bias due to cavity pulling of 1.5×10^{-17}. This bias is uncorrected and we assign the uncertainty to be 100 % of the bias.

With slight modifications to the LN_2 control system, it will be possible to reduce the cavity pulling biases by keeping the microwave cavity closer to resonance.

3.62 Rabi Pulling and Ramsey Pulling

Rabi pulling is the result of an underlying baseline slope from the m = +/-1 manifolds. Measurements of the relative amplitudes (imbalance) of these manifolds in NIST-F2 show that bias due to Rabi pulling is negligible and the fractional uncertainty in this bias is $<1 \times 10^{-17}$.

Ramsey pulling in NIST-F2 has been modeled and found to be negligible. The fractional uncertainty due to this bias is $<1 \times 10^{-17}$.

3.63 Majorana Transitions

In general, in a state-selected fountain where state-selection is performed within the magnetically shielded region, Majorana transitions are possible only after the second Ramsey interaction when the atoms have left the Ramsey interrogation region [2,28,29]. In order for a Majorana transition to cause a frequency shift a left-right (l-r) imbalance (with respect to $|F,0\rangle$) must be present. In NIST-F2 the required zero in the magnetic field and the required l-r imbalance are both absent. Additionally we use a linearly polarized detection system, thus avoiding the source of l-r asymmetry identified in [29]. We have measured the fractional m = ±1 populations after state-selection to be 6×10^{-3}, with a l-r asymmetry of 2×10^{-3} , limited by the S/N of the measurements. Given the conditions of operation of NIST-F2, this leads to a possible fractional bias from Majorana

transitions of $\delta f/f < 5 \times 10^{-18}$. We do not correct for this shift.

3.64 Resonant Light Shifts

All resonant laser light sources used for NIST-F2 reside in an adjacent laboratory and the light is delivered to the NIST-F2 via optical fiber cables. Light is attenuated during critical atom-microwave interaction intervals with a two-stage mechanical shutter and electronically by AOMs. Furthermore, light from the AOM is delivered to the physics package by additional fiber optic cables. By measuring the light attenuation factor of each stage and by operating NIST-F2 with various attenuation stages disabled, we estimate any fractional bias due to resonant light to be less than 10^{-18}, with an uncertainty of the same size.

3.65 DC Stark Shift

Cs atoms in NIST-F2 are never exposed to insulating surfaces or electrodes with applied voltages, so a bias due to the DC Stark effect is considered unlikely. An insulating area on a surface due to impurities is unlikely, given that the all copper structure was processed in a brazing furnace and standard UHV practices are used in the assembly. The only source of DC voltages is from patch-effect potentials along the microwave cavity and flight tube. Copper surfaces have varying potentials, but careful measurements [30] have shown they vary on the order of 0.01 V over spatial scales of 10^{-6} meters. An unlikely worst-case scenario would be a 0.01 V isolated surface potential as the source of a field 1 cm into the beam tube. This creates a field of only ≈1 Volt/m. If this field were located at apogee it would create a bias of $<10^{-20}$.

3.66 Background Gas Collisions

Vacuum instrumentation near the Cs source chamber in NIST-F2 indicates a pressure of 2×10^{-11} Torr. Due to the design of the vacuum system, we expect only background H_2 within the Ramsey region. First, apertures and surfaces between the Cs source chamber and the microwave cavity and time-of-flight tube are fitted with graphite getters to pump background Cs, thus reducing background Cs in the interrogation region. Finally, the cold walls (80 K) of the flight tube cryo-pump many background gases. Using published coefficients for pressure shifts due to H_2 [31] we estimate the shift due to background gases to be $<1\times10^{-17}$.

3.67 Bloch-Siegert

The fractional bias due to the Bloch-Siegert effect in NIST-F2 is estimated using equation 5.6.93b in [27] to be 2×10^{-19}, and no correction is made for this effect.

3.68 Integrator Offset

NIST-F2 uses control software that has been tested for any offsets using several methods as described in [1]. We expect no bias due to integrator offsets and assign a fractional uncertainty of 1×10^{-17}.

4. Results of NIST-F2 Accuracy Evaluation

We report the results of nine measurement campaigns of NIST-F2 from Sept 2010 to August 2013 and show in Figure 7 with respect to TAI. Included in this plot are results from NIST-F1 as well as other primary frequency standards. During this three-year period, improvements were

made on NIST-F2 aimed at improving the stability, various control systems including the LN_2 and temperature controls, software used to map the magnetic field, etc. A typical measurement campaign spanned 10 to 30 days.

Systematic biases and the associated uncertainties are shown in Table 1. During an evaluation interval NIST-F2 is operated at various atomic densities to evaluate the spin-exchange bias and at various microwave powers as part of the evaluation of microwave biases. Measurements of the DCPS that involved tilting the NIST-F2 physics package, operating at various microwave power levels while also activating opposite microwave feeds at apogee, occurred over several months in 2012.

5. Conclusion

NIST-F2 is a new primary frequency standard with a cryogenic atom interrogation region that greatly reduces the uncertainty due to the BBR shift. The Type A fractional uncertainty for the August 2013 NIST-F2 evaluation was 0.44×10^{-15} and the total Type B fractional uncertainty is 0.16×10^{-15}. The Type B uncertainty presented in this most recent evaluation is marginally larger than shown in Table 1 because the microwave amplitude effects were re-evaluated after the microwave synthesizer was slightly modified. The uncertainty due to the spin-exchange bias is included in the Type A uncertainty since it is evaluated using the statistics of the frequency measurements. The Type B uncertainty is smaller by more than a factor of two than the Type B uncertainty recently reported by the NPL-CsF2 primary frequency standard.

NIST-F2 will allow for the direct calibration of the BBR bias in the NIST-F1 primary frequency standard in future accuracy evaluations.

Acknowledgements

The authors thank Richard Fox, Tara Fortier, Mike Lombardi, and David Smith for their valuable suggestions and comments that greatly improve this paper.

Physical Effect	Magnitude	Uncertainty
Gravitational Redshift	+179.87	0.02
Second-Order Zeeman	+286.06	0.03
Blackbody Radiation	-0.087	0.005
Spin-Exchange (low density)	(-0.71)*	(0.24)*
Spin Exchange Nonlinearity	0	0.02
Microwave Amplitude Effects		
Distributed Cavity Phase Shift (DCPS)		
m=0	<0.01	<0.01
m=1	0	0.028
m=2	0	0.02
Microwave Power	<0.01	0.08
Microwave Spurious	0	0.05
Cavity pulling	0.015	0.015
Rabi pulling	<0.01	<0.01
Ramsey pulling		
Majorana transitions	<0.01	<0.01
Fluorescence light shift	<0.01	<0.01
DC Stark effect	<0.01	<0.01
Background gas collisions	<0.01	<0.01
Bloch-Siegert	<0.01	<0.01
Integrator offset	<0.01	<0.01
Total Type B Standard uncertainty		0.11

*For information purposes only. Not used in the total. See section 3.3 and [12] for details.

Table 1. The systematic biases considered for NIST-F2. Units are fractional frequency × 10^{-15}. The 2nd-order Zeeman bias is measured at regular intervals during the operation of NIST-F2. Consequently, there is no fixed value for this bias and the result here is typical. Similarly, NIST-F2 operates at a variety of atomic densities, so there is no fixed spin-exchange bias. The value given below is the spin-exchange bias at low density.

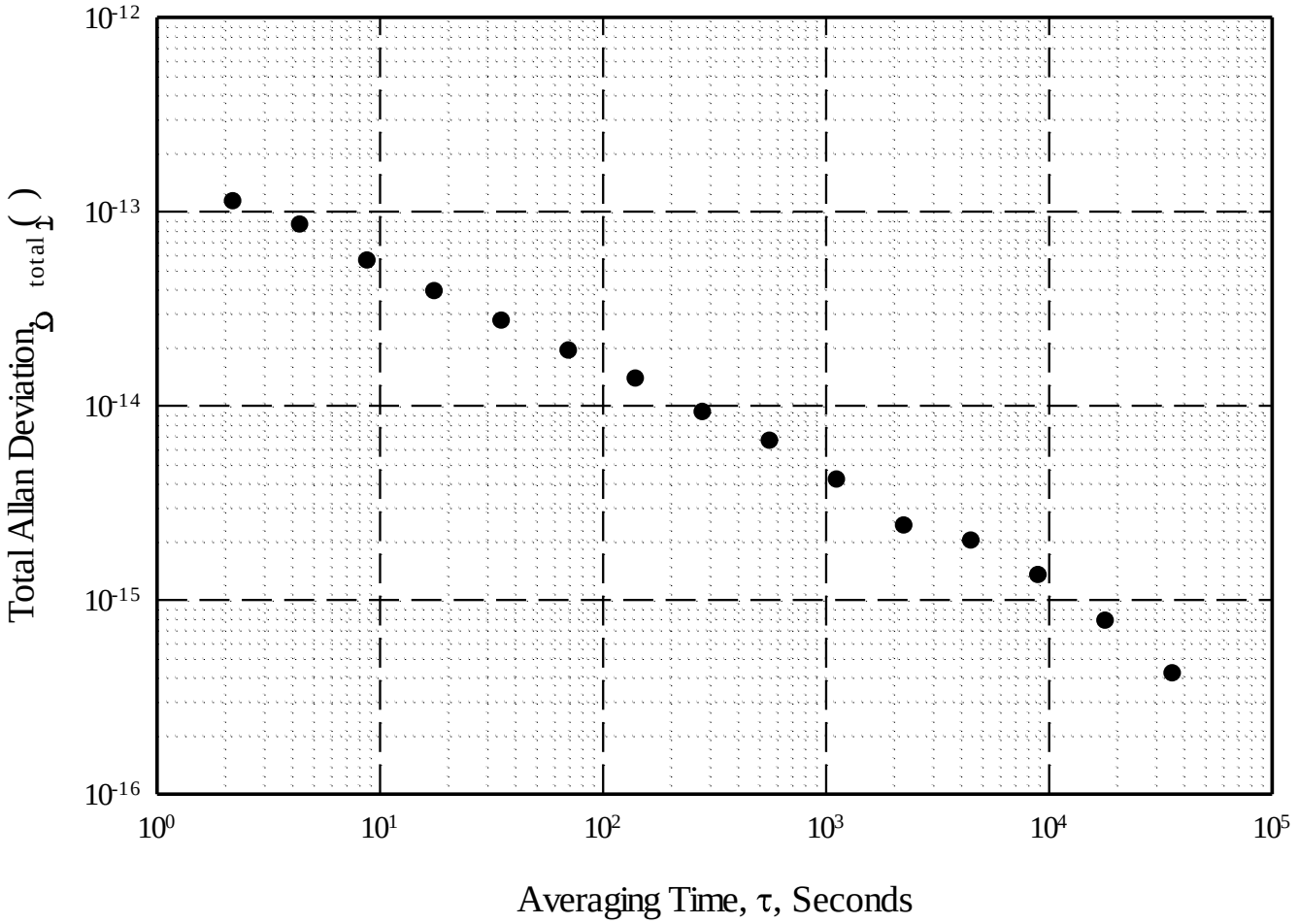

Figure 1. The Allan deviation of NIST-F2 operating at high atomic density where the stability is $\approx 1.7 \times 10^{-13}\tau^{-1/2}$.

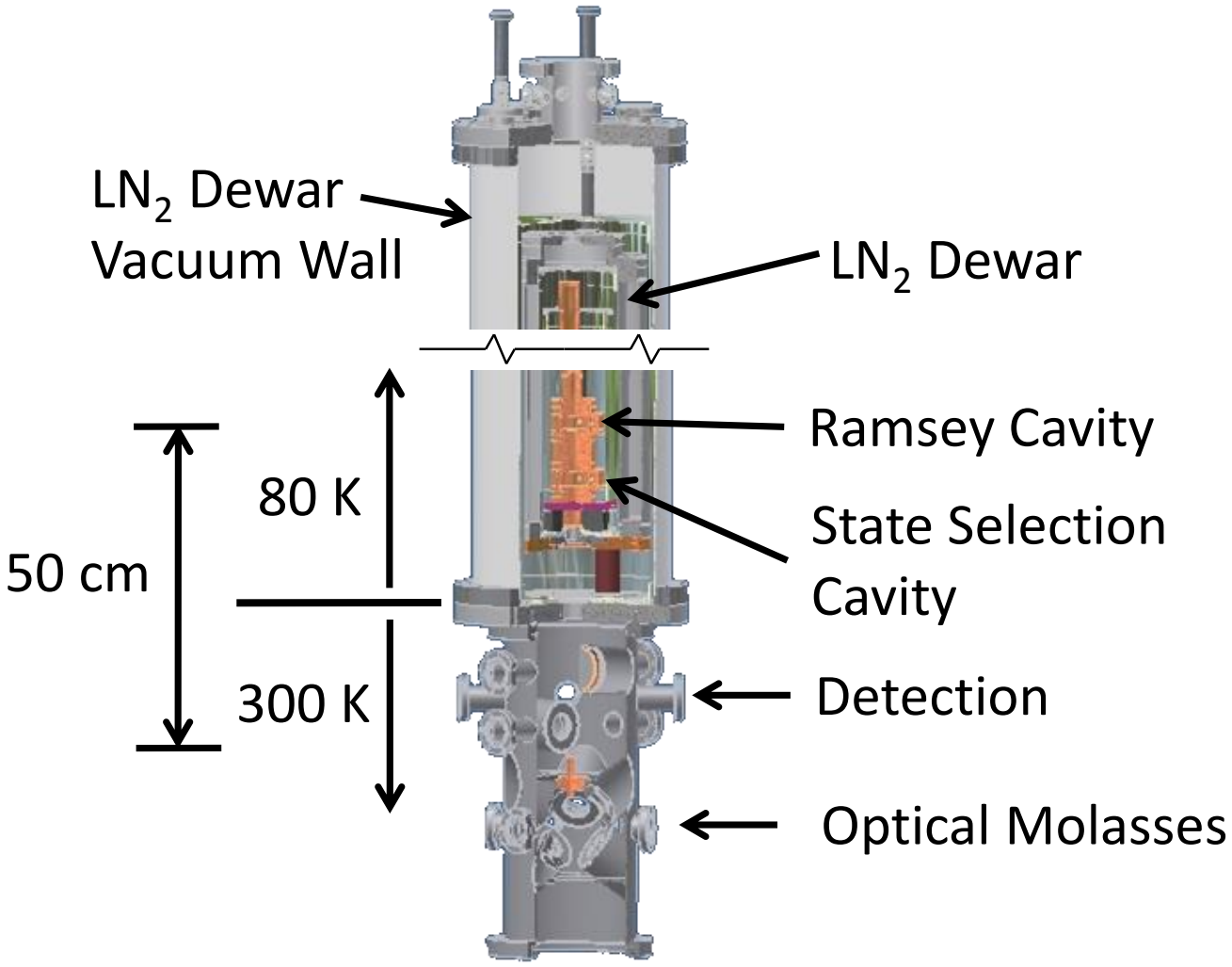

Figure 2. A Sectional View of the NIST-F2 physics package. The laser-cooled Cs source chamber operates in the (1,1,1) geometry. Directly above the source region and within the same vacuum chamber is the two-level detection zone. A short bellows with a thermal break (not shown here) connects the lower half of the system to the cryogenic microwave cavity structure. The cavity structure resides on a cold plate that is in thermal contact with the LN_2 dewar. The C-field and three layers of magnetic shields are located within the vacuum section of the LN_2 dewar. For clarity, the entire dewar structure is not shown above, but it extends approximately 1.5 m above the source/detection chamber.

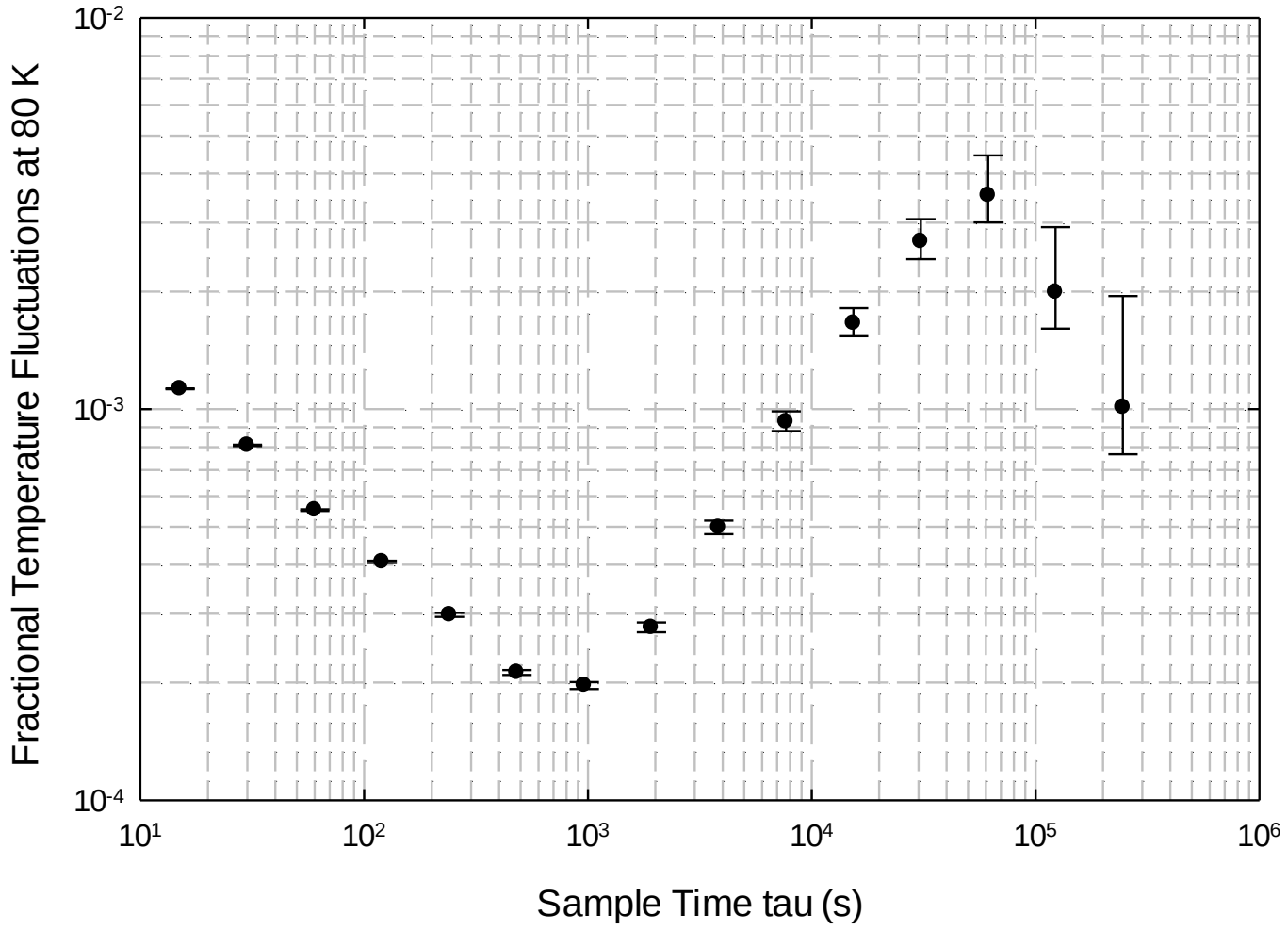

Figure 3. A plot of the Allan deviation of temperature measurements of the Ramsey microwave cavity (80 K) illustrating the long-term temperature stability.

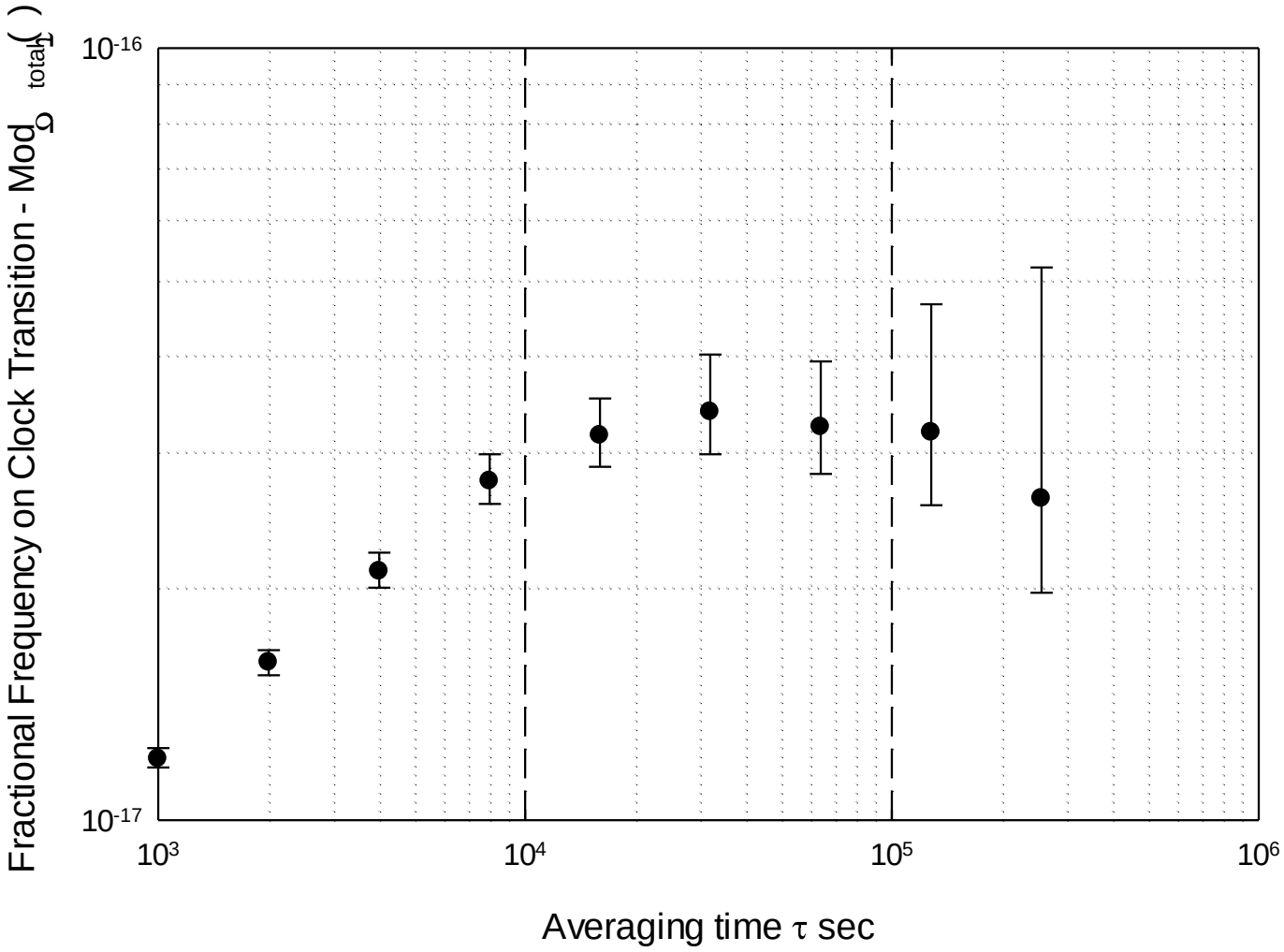

Figure 4. The Allan deviation of magnetic field measurements in NIST-F2 expressed in terms of fractional frequency fluctuations on the clock transition .

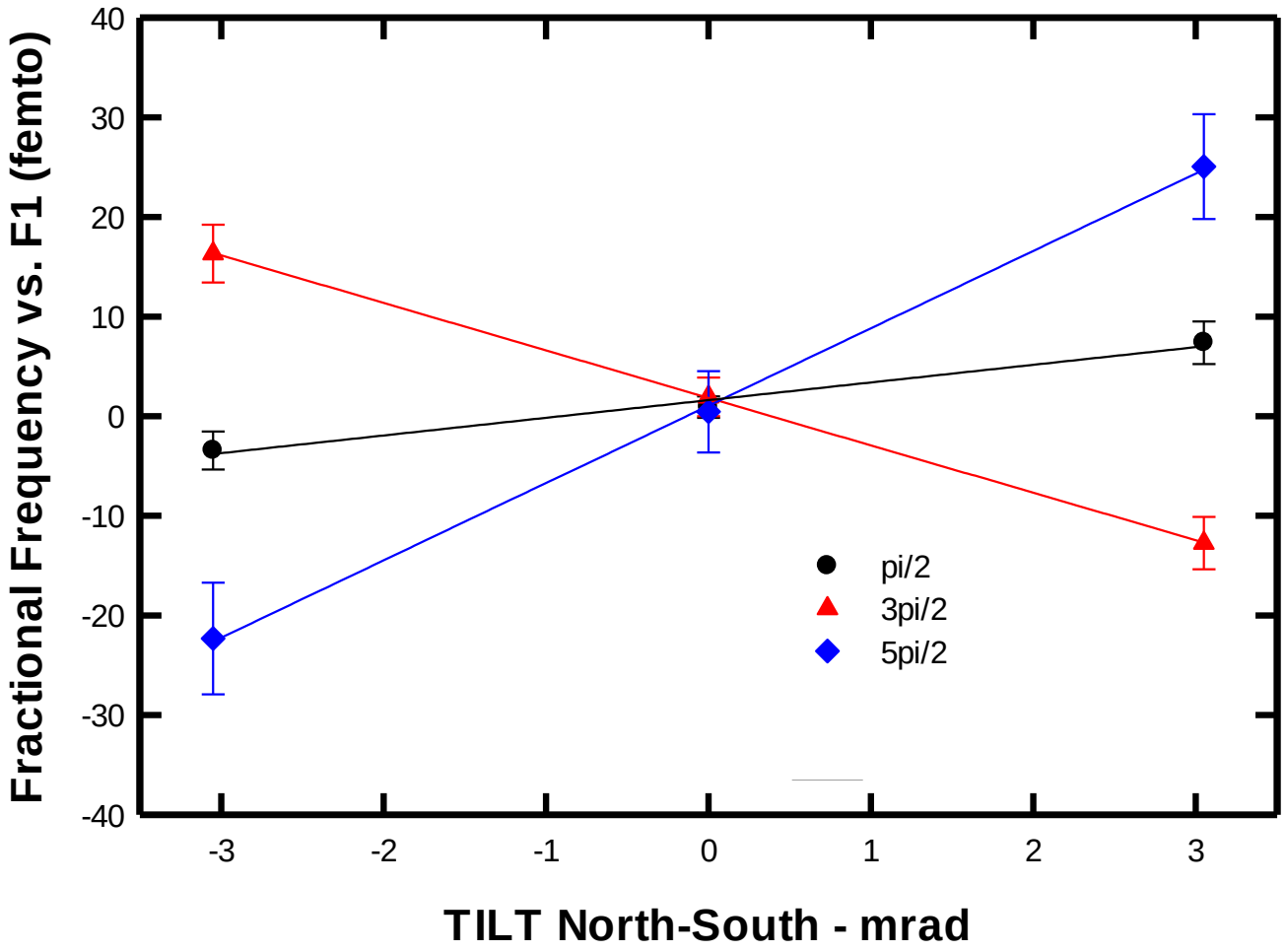

Figure 5. The measured frequency bias measured in NIST-F2 as a function of vertical tilt and microwave power. Here microwaves are introduced from alternate feeds to maximize the DCPS effect.

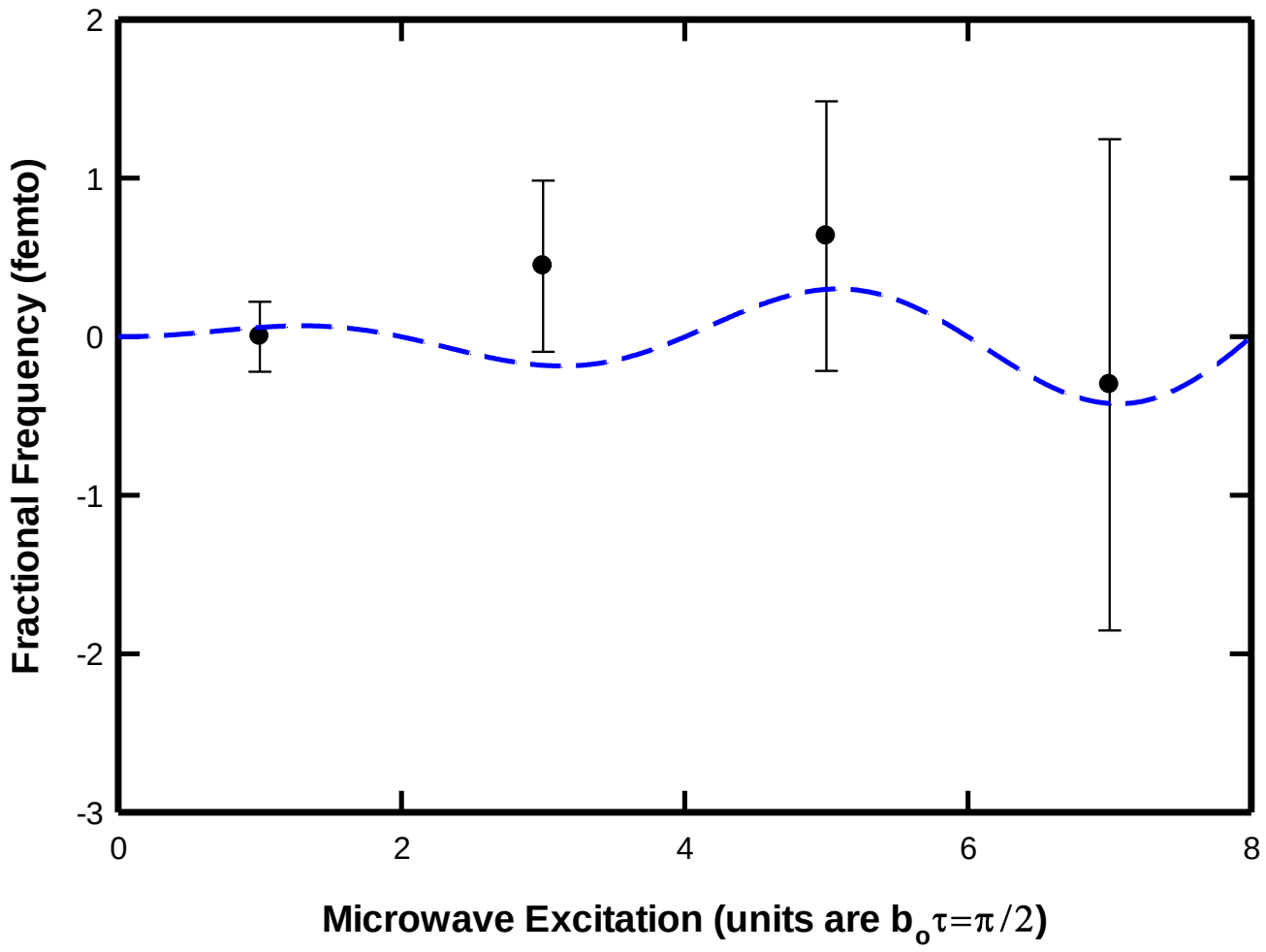

Figure 6. Fractional frequency shift of NIST-F2 as a function of Ramsey microwave power. The dotted line is a fit to Equation 2 with an amplitude given by the uncertainty in the fit.

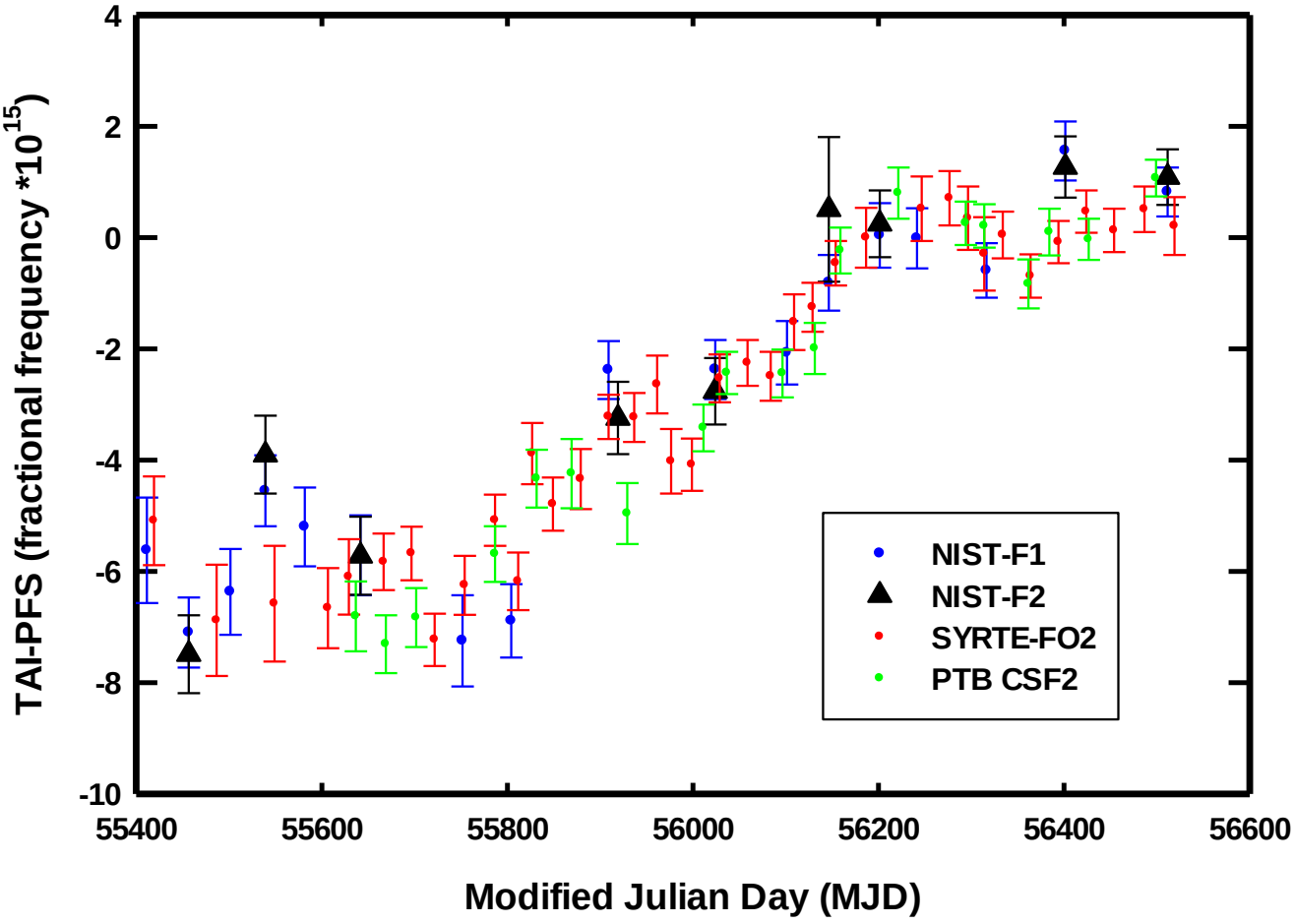

Figure 7. NIST-F2 measurements (black triangles) with respect to TAI from September 2010 to August 2013. For comparison, results from several other primary frequency standards are also shown. The most recent evaluation, August of 2013, is the first NIST-F2 accuracy evaluation submitted to the BIPM. The two NIST measurements on MJD 55539 and MJD 56401 are slightly discrepant with TAI. This is likely a time-transfer problem since NIST-F1 and NIST-F2 showed good in-house agreement.

References

[1] Heavner T P, Jefferts S R, Donley E A, Shirley J H, and Parker T E 2005 NIST-F1:recent improvements and accuracy evaluations *Metrologia* **42** 411-22

[2]Jefferts S R *et al* 2002 Accuracy evaluation of NIST-F1 *Metrologia* **39** 321-36
[3]Guéna J, Li R, Gibble K, Bize S, and Clairon A 2011 Evaluation of Doppler Shifts to Improve the Accuracy of Primary Fountain Clocks *Phys. Rev. L*ett **106** 130801
[4] Wynands R and Weyers S 2005 Atomic Fountain Clocks *Metrologia* **42** S64-S79
[5]Li R, Gibble K and Szymaniec K 2011 Improved Accuracy of the NPL-CsF2 Primary Frequency Standard:Evaluation of Distributed Cavity Phase and Microwave Lensing Frequency Shifts *Metrologia* **48** 283-289
[6]Jefferts S R, Heavner T P, Donley E A, Shirley J, and Parker T E 2003 Second Generation Cesium Fountain Primary Frequency Standards at NIST *Proc. 2003 Joint Mtg. IEEE Intl. Freq. Cont. Symp. and EFTF Conf.* 1084-1088
[7] Donley E A, HeavnerT P, O'Brien J W, Jefferts S R and Levi F 2005 Laser cooling and launching performance in a (1,1,1)-geometry atomic fountain *Proc. 2005 Joint Mtg. IEEE Intl. Freq. Cont. Symp. and PTTI* 292-296
[8], Levi F, Calosso C, Calonico D, Lorini L, Costanzo G A, Mongino B, Jefferts S R, Donley E A 2009 The Cryogenic Fountain ITCsF2 *Frequency Control Symposium, 2009 Joint with the 22nd European Frequency and Time Forum* 769-773
[9] Heavner T P, Parker T E, Shirley J H, and Jefferts S R 2008 NIST F1 and F2 *Proc. 2008 Symp. Freq. Stds. Metrology* 299-307
[10] Heavner T P, Parker T E, Shirley J H, Donley E A, Jefferts S R, Levi F, Calonico D, Calosso C, Costanzo G, and Mongino B 2011 Comparing Room Temperature and Cryogenic Cesium Fountains *Proc. 2011 Joint Mtg. IEEE Intl. Freq. Cont. Symp. and EFTF Conf.* 48-50
[11] Donley E A, Heavner T P, Levi F, Tataw M O, and Jefferts S R 2005 Double-pass Acousto-optic Modulator System *Rev. Sci. Instrum.* **76** 063122
[12] Parker T E, Jefferts S R, Heavner T P, and Donley E A 2005 Operation of the NIST-F1 caesium fountain primary frequency standard with a maser ensemble, including the impact of frequency transfer noise *Metrologia* **42** 423-430
[13] Pavlis N K and Weiss M A 2000 The relativistic redshift with $2x10^{-17}$ uncertainty at NIST, Boulder, CO USA *Proc. 2000 IEEE Intl. Freq. Cont. Symp.* 642-650
[14] Shirley J H and Jefferts S R 2003 PARCS Magnetic Field Measurement: Low Frequency Majorana Transitions and Magnetic Field Inhomogeneity *Proc. 2003 Joint Mtg. IEEE Intl. Freq. Cont. Symp. and EFTF Conf.* 1072-1075
[15]Shirley J H, Lee W D, and Drullinger R E 2001 Accuracy Evaluation of the Primary Frequency Standard NIST-7 *Metrologia* **38** 427-458
[16] Levi F, Shirley J H, Heavner T P, Yu D, and Jefferts S R 2006 Power Dependence of the Frequency Bias Caused by Spurious Components in the Microwave Spectrum in Atomic Fountains *IEEE T. Ultrason. Ferroelectr. Freq. Control* **53** 1584-1589

[17] Shirley J H, Levi F, Heavner T P, Calonico D, Yu D, and Jefferts S R 2006 Microwave Leakage-Induced Frequency Shifts in the Primary Frequency Standards NIST-F1 and IEN-CSF1 *IEEE T. Ultrason. Ferroelectr. Freq. Control* **53** 2376-2385
[18] S R Jefferts, Shirley J H, Ashby N, Heavner T P, Donley E A, and Levi F 2005 On The Power Dependence of Extraneous Microwave Fields in Atomic Frequency Standards *Proc. 2005 Joint Mtg. IEEE Intl. Freq. Cont. Symp. and PTTI* 105-110
[19] Jefferts S R, Shirley J H, Ashby N, Burt E A, and Dick G J 2005 Power Dependence of Distributed Cavity Phase-Induced Frequency Biases in Atomic Fountain Frequency Standards *IEEE T. Ultrason*. *Ferroelectr. Freq. Control* **52** 2314-2321
[20] Gibble K 2006 Difference Between a Photon's Momentum and an Atom's Recoil *Phys. Rev. Lett*. **97** 073002
[21] Ashby N, Barlow S, Jefferts S R, Heavner T P 2013 Frequency Shifts on NIST Fountains F1 and F2 Due to Transverse RF Field Gradients *to be submitted*
[22] Li R and Gibble K 2010 Evaluating and Minimizing Distributed Cavity Phase errors in Atomic Clocks *Metrologia* **47** 534
[23] Heavner T P, Jefferts S R, Donley E A, Parker T E, and Levi F 2005 A New Microwave Synthesis Chain for the Primary Frequency Standard NIST-F1 *Proc. 2005 Joint Mtg. IEEE Intl. Freq. Cont. Symp. and PTTI* 308-311
[24] Santarelli G, Governatori G, Chambon D, Lours M, Rosenbusch P, Guéna J, Chapelet F, Bize S, Tobar M, Laurent P, Portier T, and Clairon A 2009 Switching atomic fountain clock microwave interrogation signal and high-resolution phase measurements *IEEE Trans. Ultrason. Ferroelectr. Freq. Control* **56** 1319-1326
[25] Weyers S, Schröder R, and Wynands R 2006 Effects of microwave leakage in caesium clocks: theoretical and experimental results *Proc. 2006 EFTF* 173-180
[26] Bize S, Sortais Y, Mandache C, Clairon A and Salomon C 2001 Cavity Frequency Pulling in Cold Atom Fountains *IEEE Trans. Instr. and Meas.* **50** 503-506
[27] Audoin C and Vanier J 1989 *The Quantum Physics of Atomic Frequency Standards* Bristol/Philadelphia, Adam Hilger 836
[28] Bauch A, Schröder R 1993 Frequency shifts in a cesium clock due to Majorana transitions *Ann. Physik* **505** 421-449
[29] Wynands R, Schröder R, and Weyers S 2007 Majorana Transitions in an Atomic Fountain Clock *IEEE Trans. Instr. and Meas.* **56** 660-663
[30] Witteborn F C and Fairbank W M 1977 Apparatus for measuring the force of gravity on freely falling electrons *Rev. Sci. Instrum.* **48** 1-11
[31] Beer C and Bernheim R 1976 Hyperfine pressure shift of ^{133}Cs atoms in noble and molecular buffer gases *Phys. Rev. A* **13** 1052-1057